

Orbital measurement and verification of the Chandra X-Ray Observatory's PSF

D. Jerius, R.H. Donnelly, M.S. Tibbetts, R.J. Edgar, T.J. Gaetz,
D.A. Schwartz, L.P. Van Speybroeck, P.Zhao

Smithsonian Astrophysical Observatory, 60 Garden St. Cambridge Mass. 02138 USA

ABSTRACT

The recently launched Chandra X-Ray Observatory (CXO) was designed to have the sharpest angular resolution yet of any X-ray telescope. Detailed modeling and metrology of the optics followed by extensive testing at the X-Ray Calibration Facility at the Marshall Space Flight Center in Huntsville, Alabama indicated that the optics were performing exceedingly well. While our analysis accounted for distortion of the mirrors due to gravity and the effects of finite distance and size of the X-ray generator, it was only on-orbit that we expected to directly observe the specified half arc-second performance.

We present here results of the on-orbit calibration of the point spread function (PSF), comparing it with our predictions. We discuss how the PSF varies with source location in the telescope field of view, as well as with the spectral energy distribution of the source.

Keywords: X-ray optics, PSF, Chandra X-Ray Observatory, CXO

1. INTRODUCTION

The Chandra X-Ray Observatory (CXO) mirrors (the High Resolution Mirror Assembly, or HRMA) were designed to produce images with better than one arc-second resolution; in particular to concentrate better than 85% of the energy at 0.277 keV within a 1" diameter. The aggressive program put into place to ensure another, equally taxing, goal: to calibrate the optics' performance to 1%. The pursuit and attainment of these goals is the result of a collaborative effort encompassing design, fabrication, testing, and simulation.

It was recognized early on that dual tracks of laboratory calibration and systems modeling would be required to attain the program's goals. The finite resources available for laboratory measurements would preclude a thorough determination of the HRMA's performance. A substantial effort was thus directed at creating a faithful model of the HRMA's mechanical and optical systems. Ground calibration measurements were designed to test and constrain the model, which now serves as the ultimate predictor. Observations in orbit will further constrain the model, and may supplant it in certain areas.

We focus here on the testing, simulation, and final on-orbit verification of the Point Spread Function (PSF). We concentrate on three areas: the construction of the model; its predictions of the HRMA's performance during the ground calibration; and how it fares in comparison with observations made on orbit. We first look to the models to verify that the HRMA is performing within its requirements. Later we will modify the models to match the actual mirror performance.

Send correspondence to D.J.: E-mail: djerius@cfa.harvard.edu

Copyright 2000 Society of Photo-Optical Instrumentation Engineers.

This paper was published in *X-Ray Optics, Instruments, and Missions III*, Joachim E. Trümper; Bernd Aschenbach; Eds, Proceedings of SPIE Vol. 4012, p. 17, and is made available as an electronic reprint with permission of SPIE. One print or electronic copy may be made for personal use only. Systematic or multiple reproduction, distribution to multiple locations via electronic or other means, duplication of any material in this paper for a fee or for commercial purposes, or modification of the content of the paper are prohibited.

Table 1. Requirements and Predictions for on-axis CXO HRMA Performance

Incident Energy [keV]	Encircled Energy Fraction					
	1''			10''		
	Req.	Pred.	Δ	Req.	Pred.	Δ
0.28	0.88	0.79	-0.09	0.95	0.99	0.04
0.57	0.86	0.78	-0.08	0.95	0.99	0.04
0.70	0.85	0.77	-0.08	0.95	0.98	0.03
0.93	0.81	0.76	-0.05	0.95	0.98	0.03
1.49	0.72	0.75	0.03	0.92	0.97	0.05
2.98	0.50	0.70	0.20	0.81	0.96	0.15
4.95	0.29	0.65	0.36	0.67	0.93	0.26
6.40	0.22	0.65	0.43	0.62	0.94	0.32
8.04	0.20	0.57	0.37	0.59	0.92	0.33
9.18	0.17	0.55	0.38	0.57	0.91	0.34
9.71	0.15	0.54	0.39	0.55	0.90	0.35

2. OPTICS' DESCRIPTION

The CXO optics consist of four nested pairs of paraboloids and hyperboloids in a Wolter Type I design.¹⁴ The mirrors range in diameter from 0.6 m to 1.2 m, with lengths of approximately 840 mm. The system focal length is approximately 10 m. The glass (Zerodur) was figured at Hughes Danbury Optical Systems (HDOS) and coated with an iridium over chromium multilayer by Optical Coating Laboratory Inc (OCLI). The mirror assembly, consisting of the optics, their support structures, and additional thermal and optical baffles, was assembled by Eastman Kodak Co. and integrated into the telescope by TRW.

Because of the Wolter Type I design, the image quality is best in a small area centered about the optical axis. In part because the stringent design challenged current technology, the requirements on the PSF were expressed as the fraction of the total imaged energy within 1'' and 10'' diameters for an on-axis point source. They are presented in Table 1, along with predictions. These requirements are intrinsic to the mirrors, and do not include detector or aspect effects.

There are many aspects of the system which will affect the performance of the optics; the most important include:

- The optics' figure.
- The alignment of the optical elements. Misalignment within a shell manifested as either a tilt or a shift perpendicular to the optical axis will lead to an image distortion (a "tilt ring") with a diameter equal to twice the equivalent tilt.⁴ The innermost shell exhibits such a distortion, due to manufacturing alignment errors.⁶
- The roughness of the optics' surfaces. The increasingly non-specular reflection from the surface at shorter wavelengths significantly degrades performance. This is illustrated by the marked decrease in encircled energy with increased incident energy in Table 1.

3. MODELING THE OPTICS

The underlying principle in our simulation effort is to model the interaction of photons passing through the HRMA as accurately as possible. To that end we anticipated incorporating as much information as was possible about the mechanics, optics, and physics of the mirrors. The Chandra program is unlike any previous X-ray telescope missions in the extent to which varied and overwhelmingly large amounts of calibration data on the optics are available. Traditional analytical methods would have to be augmented to incorporate the data.

Our initial simulations code was derived from the Optical Surface Analysis Code (OSAC) developed for NASA by Paul Glenn² (our code has the rubric of SAOSac). We have substantially enhanced and augmented it to handle the large variety of engineering data. For instance, OSAC permitted the analysis of an optical surface defined by Fourier-Legendre polynomials. While the Chandra optics were initially modeled in this fashion, we were faced with the task

of including deformation maps based upon interferometric measurements of the optics' surfaces; we extended OSAC to allow mixing of the Fourier-Legendre description with spline interpolated maps of deviations from the nominal optics prescription. This allowed us to easily include finite-element analysis derived deformations induced by the mirror mounts as well as by gravitational perturbations present during the ground calibration.³

Enhancements were made to model surface micro-roughness scattering via zonal mirror roughness maps, based upon WYKO measurements of the optics' surfaces. We also model the reflection at the mirror surface via a multi-layer model, incorporating a Nevot-Croce treatment of the interlayer "roughness".⁷

The HRMA is composed of more than just the mirrors; the optical path through the assembly contains support structures as well as baffles and other obstructing surfaces. We have designed a flexible system⁸ to model these obstructions, allowing us to work directly from blueprints and as-built measurements.

We have developed models of the detector systems which were used during the calibration.⁶

In brief, the simulations trace photons through the optical system where they interact with the mirrors, baffles, and support structures. The mirror surface is modeled as an ideal conic surface with deformations. We model the reflectance at the iridium coated optical surface as a multi-layer model. The optical constants, layer thickness, and Nevot-Croce factors are determined from synchrotron beam measurements of witness coupons manufactured, polished, and coated to closely match the characteristics of the flight hardware.¹¹ Scattering from the iridium surface is modeled using WYKO Power Spectrum Density (PSD) measurements of the optical surfaces.⁵

The resultant simulations were used not only in the prediction of the HRMA's performance, but also in the specification and verification of the system's design. The model played a key role in the design of the measurements performed during the ground calibration; in the construction of support equipment to offset gravitational distortions of the optics' performance during those measurements; and in the design of the on-orbit calibration program.

Post-launch, the mirror model is still a very important tool, used not only to predict performance and create successful science programs, but to provide the data needed to deconvolve the mirror response from the intrinsic structures of the astrophysical sources.

When simulating performance in orbit, the flight science instruments are simulated using the MARX software package.¹⁵

4. GROUND CALIBRATION RESULTS

Pre-flight calibration of the HRMA was performed at the X-Ray Calibration Facility (XRCF) at the Marshall Space Flight Center (MSFC) in Huntsville, Alabama in the long winter months of 1996/1997. The facility consists of a large vacuum chamber in which the HRMA and detector systems were placed and a brace of X-ray sources, connected to the chamber by an evacuated tube some 524.7 m in length. A detailed description may be found elsewhere^{6,9}

There are several characteristics of the ground calibration which preclude direct comparisons with the orbital data:

- The X-ray sources were of finite extent and at a finite distance.
- The mirrors experienced distortions (squishing) due the earth's gravitational field, which was perpendicular to the optical axis. While this was compensated to a great degree by off-loading the mirrors, the effect is still visible in the data.

The performance on the ground, while still excellent compared to any other X-ray mission in orbit, is sufficiently degraded that we use the results primarily to constrain the models. We include the above effects in our simulations of the XRCF experiments.

The primary HRMA calibration was done with a specially designed instrument assembly (the HRMA X-Ray Detector System, or HXDS). The HXDS consisted of a set of instruments at the focal plane: a flow proportional counter (FPC), a germanium solid state detector (SSD), and a micro-channel plate (the High Speed Imager, or HSI) mounted on stages and equipped with pinhole apertures in a range of sizes. The throughput of the telescope was measured using a set of FPC's (the Beam Normalization Detectors, or BND's) mounted at the entrance aperture of the HRMA as well as near the X-ray sources. The spectrophotometric accuracy of the detectors was assured by absolute calibration of a subset at the BESSY synchrotron facility.⁶

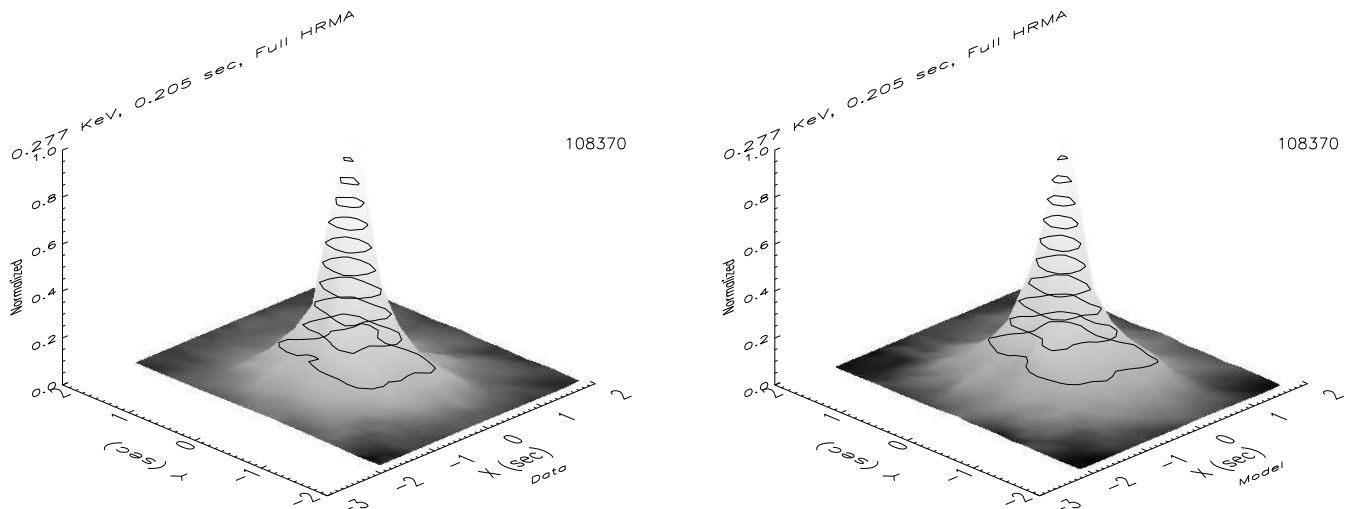


Figure 1. PSF at XRCF: 0.2'' Pinhole scans at 0.277 keV The data are to the left, the model to the right.

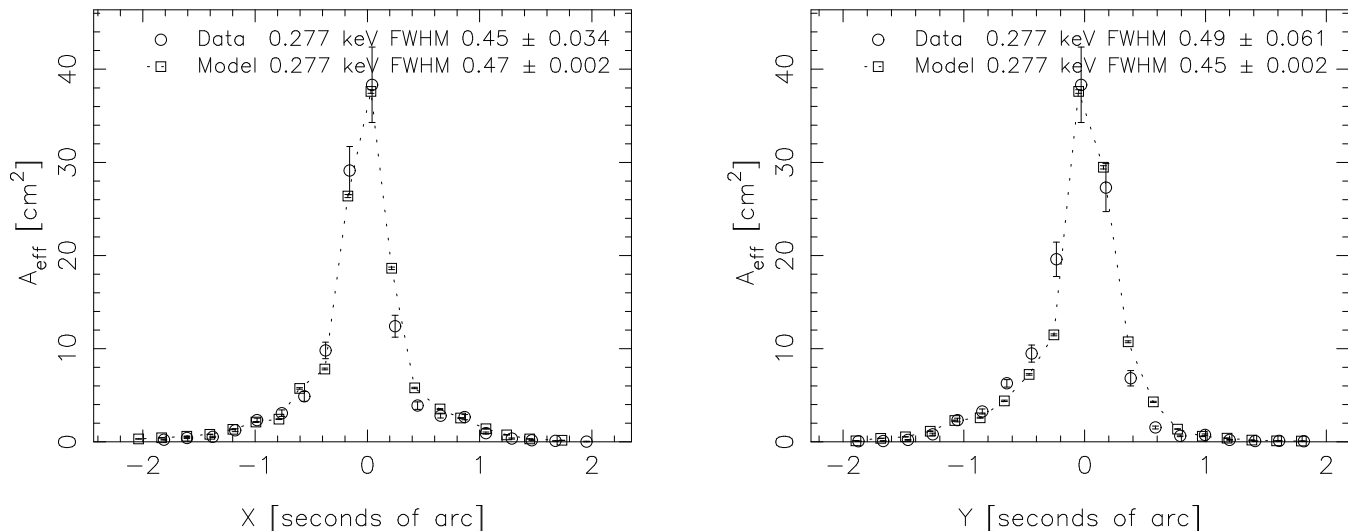


Figure 2. Cross section of the XRCF 0.277 keV pinhole scans

The precision and energy sensitivity of the HXDS detectors coupled with the spatial resolution provided by the pinholes provided the best determination of the HRMA PSF. Three classes of PSF measurements were performed:

- Two dimensional scans across the PSF using the FPC coupled with a $10\ \mu\text{m}$ (0.2'') diameter circular pinhole. These were performed on a $10\ \mu\text{m}$ grid.
- measurements of the flux with the FPC through a set of increasingly larger pinholes, essentially an encircled energy measurement.
- large aperture integration with the FPC of the PSF wings far (many minutes of arc) from the core.

Two dimensional pinhole scans and their associated simulations* are presented in Figures 1, 3, and 5. Cross sections through the peak of the effective area along perpendicular axes are shown in Figures 2, 4, and 6. It is

*The simulations were performed using `trace-xrcf2` with the `xrcf_xss_06` HRMA configuration.

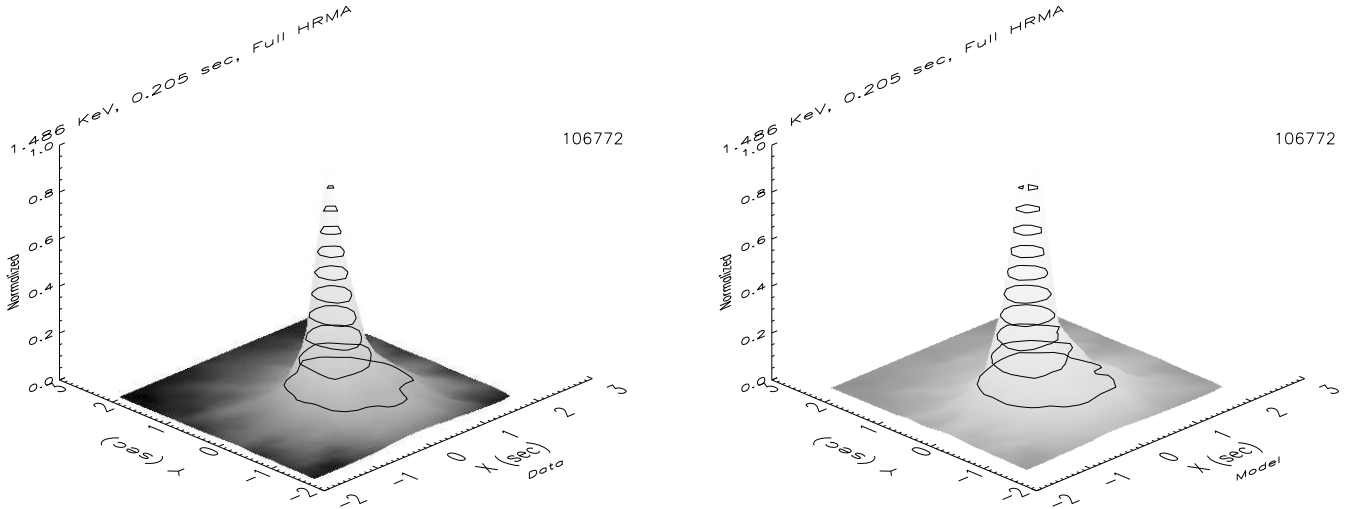


Figure 3. PSF at XRCF: $0.2''$ Pinhole scans at 1.486 keV. The data are to the left, the model to the right.

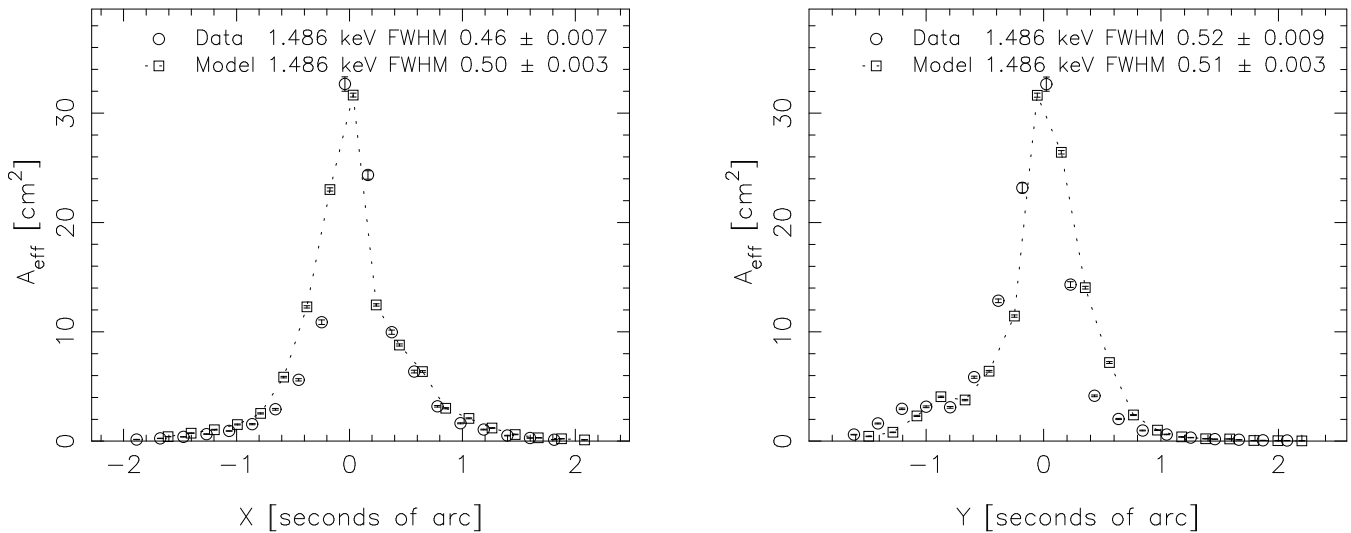


Figure 4. Cross section of the XRCF 1.486 keV pinhole scans

evident that there is good accord between the data and the model at the $0.4''$ level. The outer core (out to $1''$) is fairly well fit, with the simulations having slightly enhanced wings. The root of the remaining discrepancies has not yet been determined. At this low level, uncertainty in the systematics of the measurement process has made accurate simulation of small diameter pinhole scans quite challenging. The simulation attempts to duplicate the observation in all of its details (including the centering of the central pinhole on the peak of the beam) using the as-measured positions of the pinholes. Our simulations indicate that the model's central core does not precisely match that of the HRMA, as beam-centering the model does not lead to an identical distribution of the energy across the pinholes. The discrepancies between the model and the data on a shell-by-shell basis (which for sake of brevity are not shown here) are larger than for the full HRMA; they are averaged when combined.

The second calibration approach listed above, the measurement of the encircled energy function, is a more robust means of comparing the predictions to the data. It averages over small scale discrepancies, and requires a lesser quantity of data to achieve a statistically significant result. Its disadvantage is that it discards all of the two-dimensional structure, which will be important in resolving questions of astrophysical significance.

Figures 7 to 9 compare the encircled energy data to the simulations. Except at the highest energy, the agreement

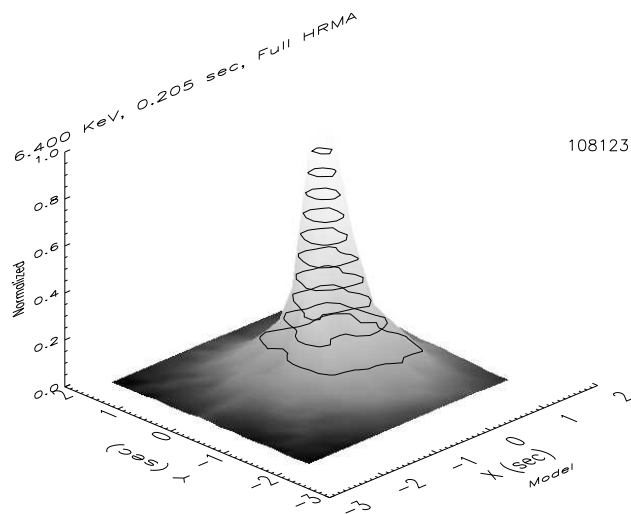
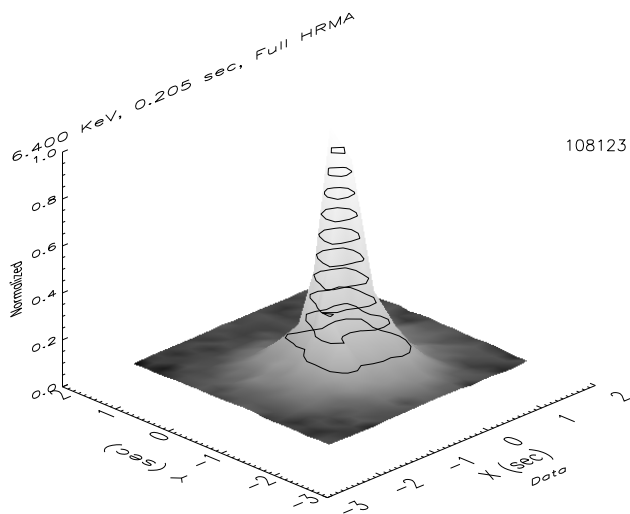


Figure 5. PSF at XRCF: 0.2'' Pinhole scans at 6.4 keV. The data are to the left, the model to the right.

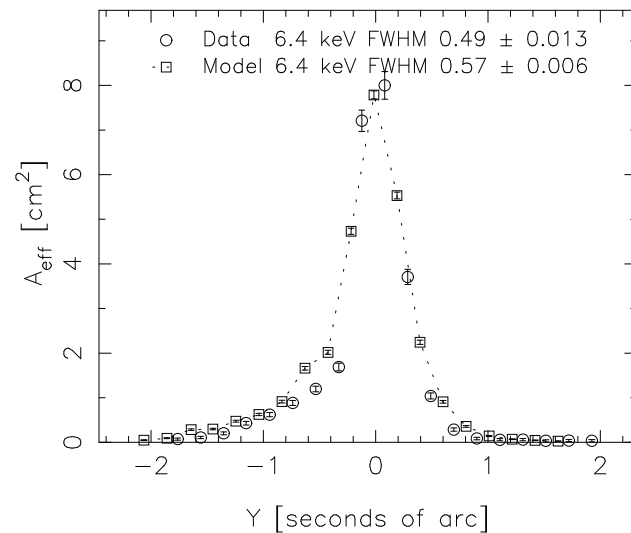
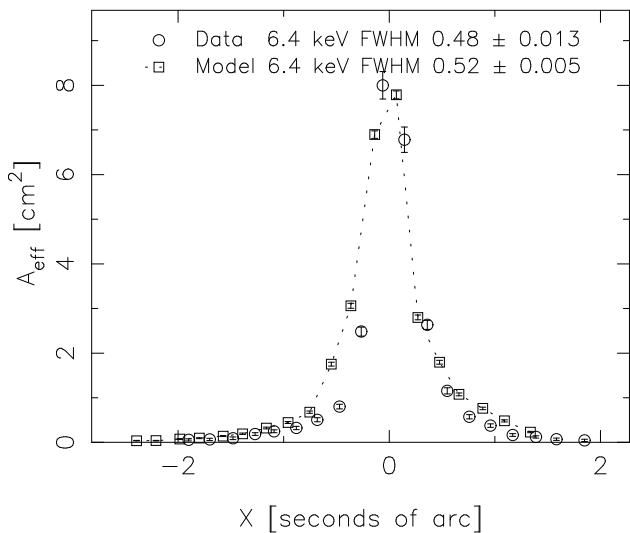


Figure 6. Cross section of the XRCF 6.4 keV pinhole scans

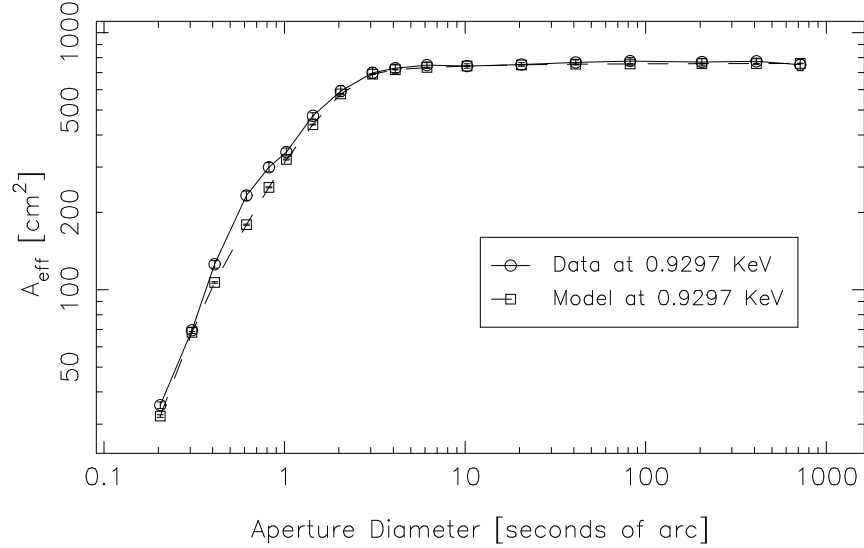


Figure 7. XRCF 0.93 keV Encircled energy.

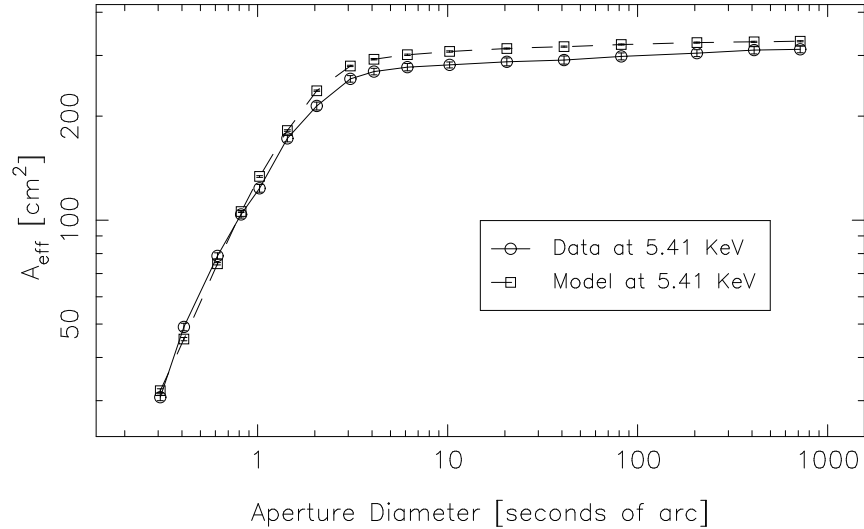


Figure 8. XRCF 5.41 keV Encircled energy.

in the core is quite good. We expect discrepancies at higher energies for two reasons:

- A slight alignment error during the assembly of the HRMA led to a tilt between the mirrors in the innermost shell (which at 8 keV is the predominant contributor to the effective area). The increased complexity of the PSF convolved with the small pinholes is difficult to accurately simulate.
- The simulations over-predict the effective area of the telescope at higher energies. The magnitude of the discrepancy is uncertain because of disagreement in the values measured independently by the FPC and SSD detectors. The SSD recorded a higher effective area than the FPC through comparably sized apertures, more in line with what the simulations predict. The encircled energy measurements presented here were performed by the FPC, as the SSD did not have large enough pinholes.⁶

There were only a few *ad hoc* modifications that needed to be made to the model to improve its predictions of the XRCF data. Not only does this indicate the soundness of its design, but gives great confidence that the model can be used to accurately predict flight performance.

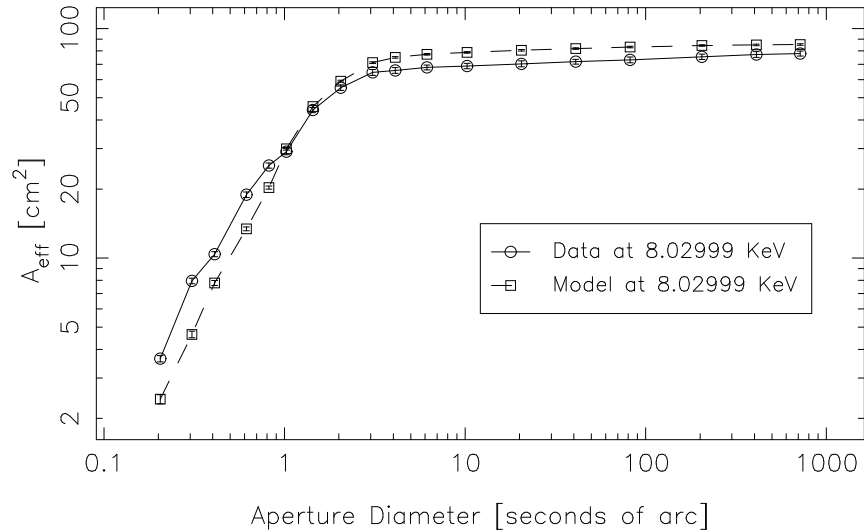


Figure 9. XRCF 8.03 keV Encircled energy.

5. ORBITAL VERIFICATION

After its launch in late Summer of 1999, Chandra went through a period of orbital activation and calibration (known as OAC). The very first image indicated that the mirrors were indeed performing better than any other X-ray telescope flown, with most of the flux from a (quite randomly selected) point source being concentrated in only a few pixels in the ACIS CCD detector (whose pixels are $0.5''$ across). Subsequent OAC images confirmed this behavior. Indeed, the object chosen to focus the telescope was discovered to have a jet separated from the main source by only a few arc-seconds [†].

Measuring the PSF on-orbit is a much more difficult task than doing so during the ground calibration. The flight PSF calibration plan is based upon parasitic monitoring, using data taken during science observations. Astrophysical X-ray sources have much lower fluxes and the science observations may be of diffuse objects. At this early stage we are limited in the quantity of data appropriate to this task; this will improve steadily over the life of the mission.

Measurements made on orbit have additional constraints (known by their more common names as the science instruments and the aspect solution) which limit our deduced knowledge of the HRMA PSF. The most suitable detector for this work is the High Resolution Camera (HRC) (a micro-channel plate detector), with an angular resolution of $\sim 0.33''$ ¹³ (*vs.* $\sim 0.5''$ for the ACIS). The aspect solution typically results in an error approximately of the same magnitude.¹

We present here results from the initial catch of calibration targets. The observations were made of AR Lac[‡], at several off-axis positions. The optics' on-orbit performance is characterized by the encircled energy function, for reasons mentioned previously. To derive the results presented below, we processed the data using standard techniques. We have used Level 1 pipeline data, and filtered the data using the `screen_hrc` tool[§]. We then fit the background. For the observations less than $5'$ from the optical axis, we have performed an additional (currently non-standard) filtering process to remove events whose positions may be displaced due to instrumental noise.¹² The remaining events preserve the angular distribution of the mirror response, but the filter removes a large percentage of the original events (up to 50%). ¶ Without the filtering, the determined on-axis 50% diameter increases from $0.76''$ to $0.84''$, while the on-axis 85% diameter increases from $1.58''$ to $1.78''$.

[†]<http://asc.harvard.edu/cal/In-Flight/Internal/jet/jet.html>

[‡]The OBSID's are 1484 1485 1486 1487 1488 1489
1491 1492 1493 1494 1495 1496 1497 1498 1499
1500 1501 1502 1503 1504

[§]<http://asc.harvard.edu/cal/Links/Hrc/CIP/filter.html>

¶The HRC instrument team and the CXC support staff are developing an algorithm which corrects for this effect; it will be introduced into the standard CXC reduction pipeline when completed and verified.

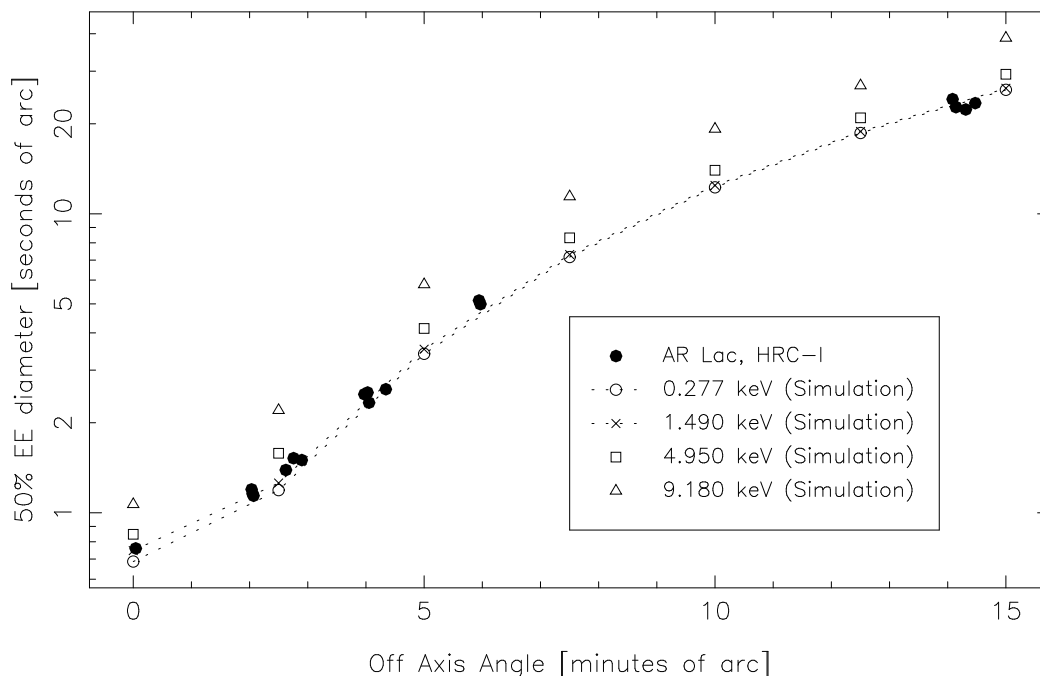


Figure 10. Observed and simulated 50% encircled energy diameters

Figures 10 and 11 show the diameters enclosing 50% and 85% of the total energy for observations of AR Lac made with the HRC-I, both on- and off- axis. The figures include simulations of the expected performance for a monochromatic point source observed with the HRC-I, with an assumed aspect error equivalent to a Gaussian with $\sigma = 0.11''$.^{||} Low statistics preclude presenting results for greater fractions of the total energy.

AR Lac is a soft source with most of its flux below 1.5 keV. The dotted lines bound the region in which its results should lie. The telescope’s performance matches the predictions remarkably well. Figure 12 presents the detailed on-axis encircled energy results. The AR Lac curve falls between the 1.49keV and 0.277 keV curves, as expected.

6. CONCLUSION

Chandra’s mirrors are performing remarkably well. The PSF, as measured by the encircled energy, is in excellent agreement with that indicated by the models. The models have thus been shown to accurately predict the PSF.

These results are very heartening, but are limited by their one-dimensional nature. We expect to be able to perform more sophisticated two-dimensional analyses as the catalogue of objects appropriate to this analysis grows. Future work will include observations by the ACIS detector, which, because of its spectral sensitivity, will allow us to separate out the energy dependent characteristics of the PSF.

ACKNOWLEDGMENTS

The authors acknowledge support for this research from NASA contract NAS8-39073.

REFERENCES

1. T. Aldcroft, M. Karovska, M. Cresitello-Dittmar, R. Cameron, “Initial performance of the aspect system on the Chandra Observatory: post-facto aspect reconstruction,” *Proc. SPIE* **4012**, this volume (2000).
2. P.Glenn, “Optical Surface Analysis Code: Final Report,” Perken-Elmer Optical Technology Division Engineering Report ER-527, (1982).

^{||}The simulations were performed using `trace-nest2` with the `orbit_XRCF_tilts_02` HRMA configuration. MARX version 2.21 was used to model the HRC-I. The aspect error was introduced by convolving the rays with a Gaussian of the specified width before they interacted with the detector.

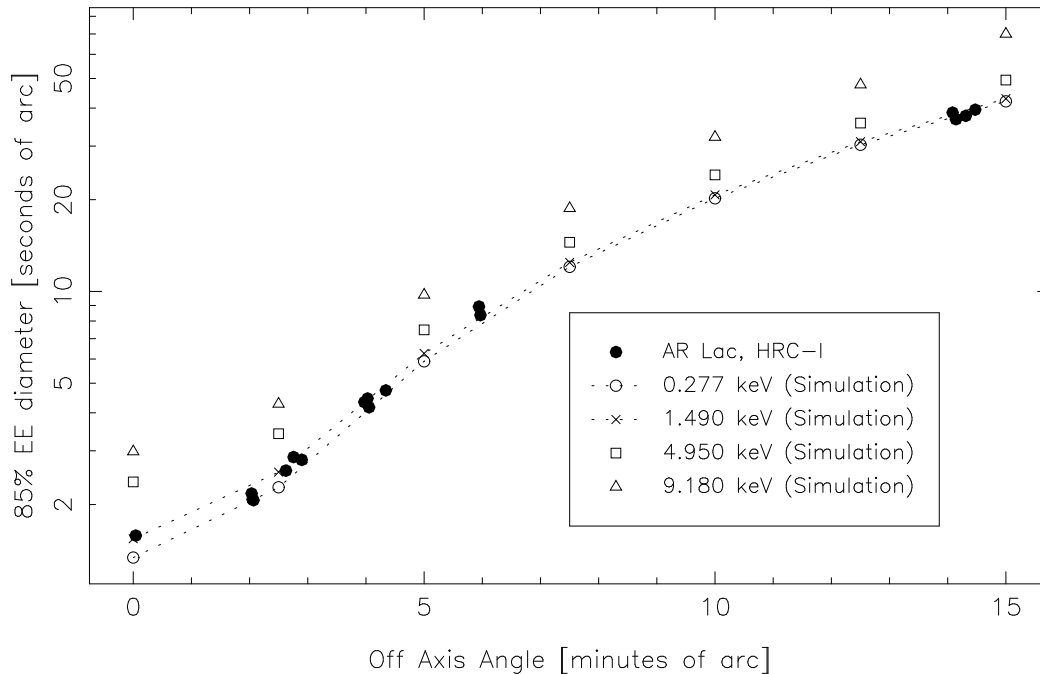


Figure 11. Observed and simulated 85% Encircled Energy Diameters.

3. D. Jerius, M. Freeman, T. Gaetz, J.P. Hughes, and W. Podgorski, "The SAO AXAF Simulation System," in *ADASS IV, ASP Conference Series*, **77**, pp. 357-360 (1995).
4. D. Jerius, J.P. Hughes, "HMRA Calibration Handbook: EKC Gravity Compensated XRCF Models," Smithsonian Astrophysical Observatory Performance Report, SAO-AXAF-DR-94-088 (1994).
5. D. Jerius, J.P. Hughes, "HRMA Calibration Handbook: Volume II - AXAF Specification Mirror Performance," Smithsonian Astrophysical Observatory Performance Report, SAO-AXAF-DR-95-144 (1995).
6. D. Jerius, editor, "XRCF Phase 1 Testing: Analysis Results," Smithsonian Astrophysical Observatory Performance Report <http://hea-www.harvard.edu/MST/simul/xrcf/report/index.html> (2000).
7. L. Nevot and P. Croce, *Rev. Phys. Appl.* **15**, p 761 (1980).
8. D. Nguyen, T. Gaetz, D. Jerius, I. Stern, "Modeling AXAF Obstructions with the Generalized Aperture Program," *ADASS VI, A.S.P. Conference Series*, **125**, p. 485 (1997).
9. D.A. Schwartz, L.P. David, R.H. Donnelly, R.J. Edgar, R.J. Gaetz, D. Jerius, M. Juda, E.M. Kellogg, B.R. McNamara, P.P. Plucinsky, L.P. Van Speybroeck, B.J. Wargelin, S. Wolk, P. Zhao, D. Dewey, H.L. Marshall, N.S. Schulz, R.F. Elsner, J.J. Kolodziejczak, S.L. O'Dell, D.A. Swartz, A.F. Tennat, M.C. Weisskopf, "Absolute effective area of the Chandra High Resolution Mirror Assembly," *Proc. SPIE* **4012**, this volume (2000).
10. T.J. Gaetz, D. Jerius, R.J. Edgar, L.P. Van Speybroeck, D.A. Schwartz, M. Markevitch, N.S. Schulz, "Orbital Verification of the CXO High Resolution Mirror Assembly Alignment and Vignetting," *Proc. SPIE* **4012**, this volume (2000).
11. D.E. Graessle, A.J. Burek, J.J. Fitch, B. Harris, D.A. Schwartz, and R.L. Blake, "Optical constants from synchrotron reflectance measurements of AXAF witness mirrors, 2-12keV," *Proc. SPIE* **3113**, pp 52-64 (1977).
12. A. Kenter, J.H. Chappell, R. Kraft, G. Meehan, S.S. Murray, M. Zombeck, K.T. Hole, M. Juda, R.H. Donnelly, D. Patnaude, D. Pease, C. Wilton, P. Zhao, G. Austin, "In-flight Performance and Calibration of the Chandra High Resolution Camera Imager (HRC-I)," *Proc. SPIE* **4012**, this volume (2000).
13. S.S. Murray, G.K. Austin, J.H. Chappell, J.J. Gomes, A.T. Kenter, R.P. Kraft, G.R. Meehan, M.V. Zombeck, G.W. Fraser, S. Serio, "In-flight performance of the Chandra High Resolution Camera," *Proc. SPIE* **4012**, this volume (2000).
14. L. P. Van Speybroeck, and R. C. Chase, "Design Parameters of Paraboloid-Hyperboloid Telescopes for X-ray Astronomy," *Applied Optics*, **11**, 2, pp. 440-445.

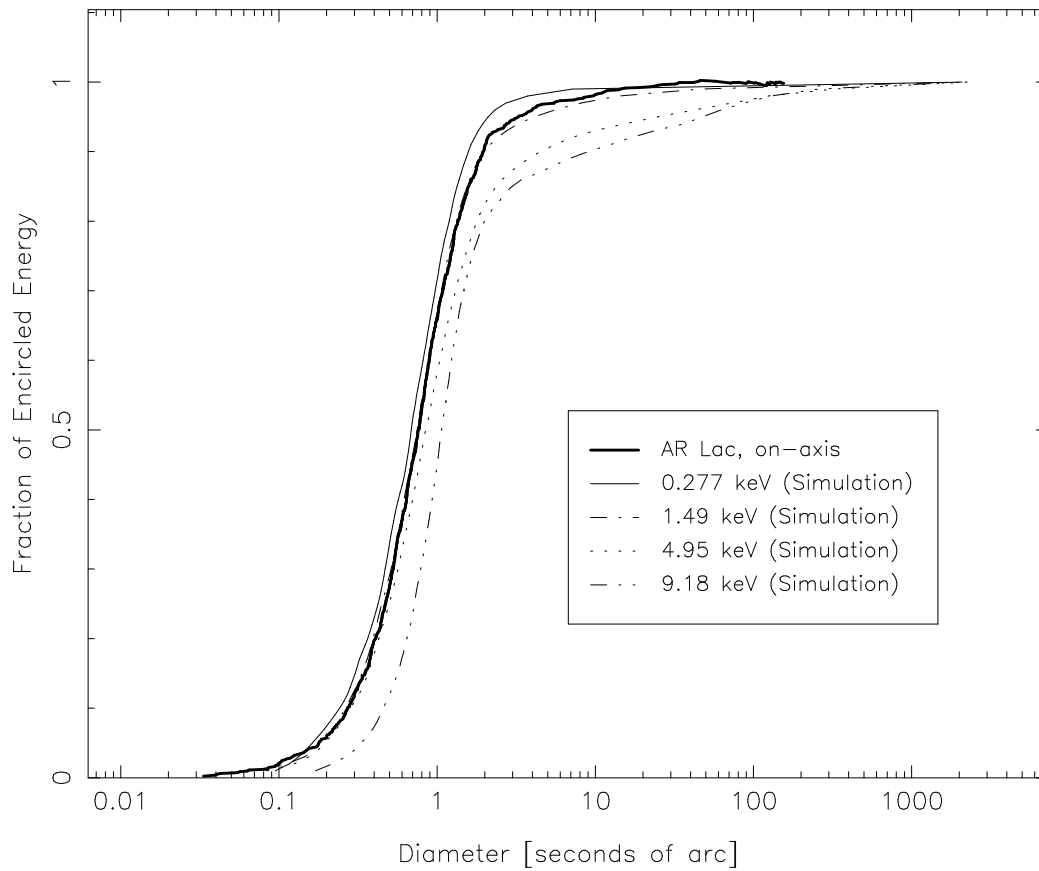


Figure 12. The detailed encircled energy data for the on-axis AR Lac observation, compared to simulations of monochromatic point sources with the specified energies.

15. M.W. Wise, J.E. Davis, D.P. Huenemoerder, J.C. Houck, D. Dewey, K.A. Flanagan, and C. Baluta, "The MARX 2.0 User Guide," AXAF Science Center Technical Document 404 (1997).